A&A, 713, A131 (2026)
https://doi.org/10.1051/0004-6361/202659807

Astronomy & Astrophysics

Universal behaviour of α-viscosity in black hole accretion discs

Marek A. Abramowicz[1,2,3,⋆], Axel Brandenburg[4,5], Jiří Horák[6], Debora Lančová[2,3,⋆], John C. Miller[7,8], Ewa Szuszkiewicz[9], and Maciek Wielgus[10]

1 Physics Department, Gothenburg University, SE-412-96 Göteborg, Sweden
2 Nicolaus Copernicus Astronomical Center, Polish Academy of Sciences, Bartycka 18, PL-00-716 Warszawa, Poland
3 Research Center for Computational Physics and Data Processing, Institute of Physics, Silesian University in Opava, Bezručovo nám. 13, CZ-746 01 Opava, Czech Republic
4 Nordita, Hannes Alfvèns väg 12, SE-106 91 Stockholm, Sweden
5 The Oskar Klein Centre, Department of Astronomy, Stockholm University, AlbaNova 10691, Stockholm, Sweden
6 Astronomical Institute of the Czech Academy of Sciences, Boční II 1401/1a, CZ-141 31 Praha 4, Czech Republic
7 Department of Physics (Astrophysics), University of Oxford, Keble Road, Oxford OX1 3RH, United Kingdom
8 International School for Advanced Studies, SISSA, Via Bonomea 265, 34136 Trieste, Italy
9 Institute of Physics and CASA*, University of Szczecin, ul. Wielkopolska 15, PL-70-451 Szczecin, Poland
10 Instituto de Astrofísica de Andalucía-CSIC, Glorieta de la Astronomía s/n, E-18008 Granada, Spain

Received 11 March 2026 / Accepted 6 July 2026

ABSTRACT

The Shakura-Sunyaev α-viscosity coefficient, defined as the ratio of total stress to total pressure, $\alpha = \mathbb{T}/p$, began to play an important role in the development of accretion disc theory in the early 1970s. The origin of the turbulence that causes the stress, $\mathbb{T}$, was unknown at that time; Shakura and Sunyaev assumed α = const. Today we know that this was not very realistic – modern general relativistic magneto-hydrodynamics (GRMHD) simulations of black hole accretion discs have revealed that α changes by about an order of magnitude within the disc, being smaller far away from the black hole and larger in the plunging region close in, and it has been found that the behaviour of α reflects some underlying, fundamental properties of the stress, $\mathbb{T}$. In particular, it has been argued by several authors, that $\mathbb{T}$ must be zero at the black hole horizon. We note that the stress as calculated in three independent GRMHD simulations of accretion discs around non-rotating black holes, made by a variety of authors (including ourselves), always has its prominent maximum close to the location of the circular photon orbit. We propose a formula that accurately describes this 'universal' behaviour of α in terms of the 'gyration radius', a physical characteristic of rotation well known in Newtonian dynamics and, in the black hole case, uniquely defined by the Kerr space-time geometry. Analytic and semi-analytic models of black hole accretion discs provide an invaluable insight into fundamental physics, and the GRMHD simulations do not aspire to replace them. Rather, simulations could help to improve analytic models by making them more realistic. For example, our α-formula, deduced from the GRMHD simulations, may be useful in the construction of improved versions of thin and slim disc models.

Key words. accretion, accretion disks – black hole physics – magnetohydrodynamics (MHD) – turbulence

1. Introduction

The classic, analytic model by Shakura & Sunyaev (1973) remains one of the pillars on which our understanding of the fundamental physics governing black hole accretion discs rests. The remarkable practical usefulness of the model results from its sharp clarity that was achieved thanks to several brilliant assumptions that were made. Perhaps the most important of them is the treatment of the 'viscous' stress $\mathbb{T}$ that powers the accretion disc's radiation by enhancing angular momentum transport and dissipating orbital energy of matter into heat. Directly from the fundamental conservation laws, Shakura & Sunyaev (1973) derived equations for the radial fluxes of mass ($\dot{M}$), angular momentum ($\dot{J}$), and energy ($\dot{E}$) in accretion discs:

$$\dot{M} = \int_{-H}^{+H} 2\pi r \, \rho v \, dz, \tag{1}$$

$$\dot{J} = \dot{M}\, j + \mathbb{T}, \quad \dot{E} = \dot{M}\, e + \Omega\mathbb{T}. \tag{2}$$

Here, ρ is the mass density, v is the radial velocity of the matter, j and e are the specific (per mass) angular momentum and energy, and Ω is the angular velocity[1]. The integration goes through the disc vertical thickness:

$$z = H(r), \quad z = r\cos(\theta). \tag{3}$$

For each of the three fluxes $\dot{M}$, $\dot{J}$ and $\dot{E}$, the differences between their values at successive radial locations r_1 and r_2 are:

$$\Delta\dot{M} = 0, \quad \Delta\dot{J} = 0, \quad \Delta\dot{E} = \int_{r_2}^{r_1} F \, 2\pi r \, dr. \tag{4}$$

The radial flux of energy is not constant because energy is also partially radiated from the disc; F denotes the flux of energy that is locally radiated. From Eqs. (1)–(4), Shakura & Sunyaev

⋆ Corresponding authors: marek.abramowicz@physics.gu.se; debora.lancova@gmail.com

1 For simplicity we consider here a Schwarzschild black hole and use spherical coordinates $\{t, r, \theta, \phi\}$ and a metric signature $(+, -, -, -)$, in which $g_{tt} = c^2(1 - r_{\rm H}/r)$ and $g_{\phi\phi} = -\sin^2(\theta)\, r^2$ with $r_{\rm H} = 2\,GM/c^2$ being the horizon location and M being the mass of the black hole. The Kerr black hole formulae are given in the Appendix A.

(1973) derived that the flux is given by

$$F = \frac{\dot{M}}{4\pi r}\left(\frac{d\Omega}{dr}\right)\left[j\left(r\right) - j\left(r_0\right)\right], \tag{5}$$

where $j(r)$ is the radial angular momentum distribution in the disc and r_0 is the radial location of the place where the stress is zero, $\mathbb{T}(r_0) = 0$. Note that

$$j = \Omega\tilde{r}^2 \quad \tilde{r} = \left(-\frac{g_{\phi\phi}}{g_{tt}}\right)^{1/2} = \text{gyration radius}. \tag{6}$$

Knowing r_0 and $j(r)$, and therefore also $\Omega(r)$, suffices to calculate the local radiation flux from Eq. (5).

For a razor thin disc, $h = H/r \ll 1$, one may assume, with accuracy to linear order terms $O^1(h)$, that

$$j(r) = \left\{\begin{array}{ll} j_K(r) = \tilde{r}^2\Omega_K(r) & \text{if } r > r_0 \\ j_K(r_0) = \text{const} & \text{if } r < r_0 \end{array}\right\}, \tag{7}$$

where $\Omega_K(r)$ is the Keplerian angular velocity and r_0 is the location of the innermost stable circular orbit (ISCO). Because $\Omega_K(r)$ and the location of the ISCO are known analytically in the Kerr geometry from Eq. (7), one can derive the formula for the radiation flux emitted in an explicit (and very simple) form. Its Newtonian version is

$$F(r) = \frac{3GM\dot{M}}{8\pi r^3}\left[1 - \sqrt{\frac{r_0}{r}}\right], \quad r_0 = \frac{6GM}{c^2}. \tag{8}$$

Formulae (5) and (8) are undoubtedly the most famous and useful in accretion disc theory. They have been used in Newtonian, Schwarzschild, and Kerr versions by numerous authors to calculate the observational appearance of accretion discs (e.g., Novikov & Thorne 1973). They do not depend on the stress ($\mathbb{T}$), and this was an enormous benefit in the early days of the development of the theory, when the nature of the stress was unknown. Because the stress enters a few other equations on which their model rests, Shakura & Sunyaev (1973) adopted an ansatz known as the Shakura-Sunyaev viscosity prescription, which states that the stress is proportional to the total pressure,

$$\mathbb{T} = \alpha p, \quad \alpha = \text{const}. \tag{9}$$

There is a problem here. Formula (8) is valid only in the limit of a razor thin disc $h \to 0$, when only the lowest-order terms ($\sim O^1[h]$) are taken into account. When the disc luminosity is greater than about $\sim 0.3\, L_{\rm Edd}$, where $L_{\rm Edd}$ is the Eddington luminosity[2], several important physical effects, in particular the radial advection of heat described by the $O^2[h]$ terms, must be taken into account because they qualitatively change the physics of accretion. In particular, neither $j(r) = j_K(r)$ nor $\mathbb{T}(r_{\rm ISCO}) = 0$ is valid.

The slim disc model (Abramowicz et al. 1988), comprehensively discussed in Sądowski (2009), incorporates all of the $O^2[h]$ terms that are missed in the thin disc model. In slim discs the stress is zero, not at the ISCO, but at the horizon $r_{\rm H}$ and, correspondingly, the constant $j_0 = j(r_0)$ that appears in formula (5) does not equal $j_K(r_{\rm ISCO})$ as in thin discs, but instead is an eigenvalue of the problem, not known a priori. It cannot be assumed, but should be self-consistently calculated from the (extra) condition of regularity at the sonic radius, $r_{\rm S}$. Formula (5) only seemingly does not depend on the stress. In fact, when the terms $O^2[h]$ are included, it depends strongly through the angular momentum distribution, $j(r)$, which is directly governed by the stress. For this reason, in the plunging region of slim discs, located between the sonic radius and the horizon, $r_{\rm H} < r < r_{\rm S}$, the angular momentum is not constant and, correspondingly, the radiation flux, $F(r)$, is not zero but can be quite large, as calculations by Sądowski (2009) have clearly demonstrated.

Obviously, the exact knowledge of the stress in the plunging region is important for calculating the radiation flux, $F(r)$. Because slim disc models use the classic Shakura-Sunyaev ansatz for the stress (Eq. (9)), the currently used slim disc values of $F(r)$ are not realistic. A more sophisticated description of the stress in slim discs is needed.

The importance of the plunging region emission has been recognised by many authors in both analytical and numerical studies (Krolik & Hawley 2002; Shafee et al. 2008; Penna et al. 2010; Morales Teixeira et al. 2018; Hankla et al. 2022; Mummery & Balbus 2023). It was also demonstrated that the plunging region emission is important for the spin estimation in black hole binaries (e.g., Reynolds 2021; Wielgus et al. 2022; Mummery et al. 2025; Dhang et al. 2025; Zdziarski et al. 2026). In those works, when a viscosity prescription is adopted, α is assumed to be constant throughout the disc, including in the plunging region. Our formula extends this prescription by adopting a more physically motivated radial dependence of α, with vanishing stress at the black hole horizon (as in slim discs) and with a maximum at the photon orbit, which more accurately reflects the behaviour of the accreting gas and magnetic fields in the vicinity of the event horizon.

2. Our α-prescription formula

We suggest that the Shakura-Sunyaev constant α-prescription formula (9) should be replaced by[3]

$$\alpha = \alpha(r) = \left[\alpha_P\left(\frac{r_{\rm H}}{r}\right)^2 + \alpha_\infty\right]\left(1 - \frac{r_{\rm H}}{r}\right), \tag{10}$$

with α_P and α_∞ being two phenomenological constants: $\alpha_P = 4.71$ and $\alpha_\infty = 0.01$ give the best fit to the simulations by Lančová et al. (2026), denoted as L26 in this work; see Figure 1.

The coordinate-independent version of Eq. (10), written with the help of the Killing vector η^ν (which describes the Schwarzschild metric time symmetry) and the Killing vector ξ^ν (axial symmetry) is[4]

$$\alpha = \alpha_P\left(\frac{r_{\rm H}}{\tilde{r}}\right)^2 + \alpha_\infty\,(\eta\eta)\,. \tag{11}$$

We use the notation $(\xi\xi) = \xi^\mu\xi^\nu g_{\mu\nu}$, and likewise for $(\eta\eta)$.

The 'gyration radius' ($\tilde{r}$) is a key element in the arguments presented in this paper,

$$\tilde{r} = \left[-\frac{(\xi\xi)}{(\eta\eta)}\right]^{1/2}. \tag{12}$$

In Newtonian dynamics for a single particle orbiting a circle, the gyration radius is just the radius of the orbit, whilst for rotating solids, the gyration radius relates to the moments of inertia. Abramowicz et al. (1993) discussed in detail its physical meaning in terms of Einstein's general relativity. As in Newtonian

[2] The corresponding mass accretion rate is $\dot{M}_{\rm Edd} = L_{\rm Edd}/(\eta_{\rm NT}c^2)$, where $\eta_{\rm NT}$ is the Novikov & Thorne (1973) accretion efficiency.

[3] In the case of accretion discs around a non-rotating Schwarzschild black hole; see footnote 1.

[4] In Appendix A, we give the Kerr metric formulae.

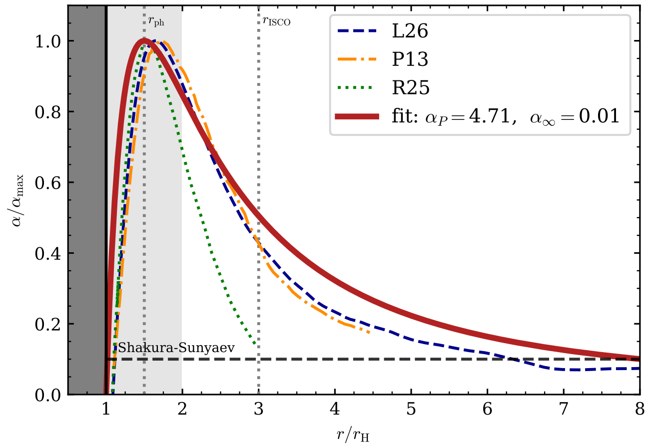

Fig. 1. The α-viscosity coefficient calculated in GRMHD simulations by L26, Penna et al. (2013), denoted by P13, and Rule et al. (2025), denoted by R25, all for accretion discs around non-rotating black holes, fitted to our α-prescription formula (Eq. (11)). Three characteristic features are visible in all of the simulations: [1] $\alpha = 0$ at the horizon $r = r_H$, [2] α has a maximum very close to the location of the circular light ray at $r_{ph} = (3/2)\, r_H$, [3] for large radii $r \gg r_H$, α is much smaller than in the plunging region. The plunging region is located between the sonic radius r_S and the horizon r_H and is highlighted by the light grey colour (r_S is taken from L26). All curves are normalised by their respective maxima: $\alpha_{max} = 0.8$ for L26, 0.3 for P13, and 0.3 for R25. Since R25 uses only the Maxwell stress in the local fluid frame (see Section 3), their α definition is mostly valid in the highly magnetised plunging region and we therefore only show R25 data up to r_{ISCO}.

dynamics, in Einstein's relativity for a particle with four-velocity u^ν in the Schwarzschild space-time, the specific angular momentum $j = -u_\phi/u_t$ and the angular velocity $\Omega = u^\phi/u^t = d\phi/dt$ are related by Eq. (6).

The first term in Eq. (11) dominates near to the black hole and far away it tends to zero. The second term dominates far away; it is introduced in order to reflect the asymptotic behaviour of α at large radii.

3. Stress calculated from GRMHD simulations

3.1. General remarks

In the GRMHD simulations of black hole accretion discs one usually assumes that the total stress-energy tensor is the sum of the Reynolds and Maxwell components,[5]

$$T^{\rm Tot}_{\mu\nu} = T^{\rm Rey}_{\mu\nu} + T^{\rm Max}_{\mu\nu}, \tag{13}$$

$$T^{\rm Rey}_{\mu\nu} = \varepsilon\, u_\mu u_\nu + p_{\rm gas} g_{\mu\nu}, \tag{14}$$

$$T^{\rm Max}_{\mu\nu} = b^2 u_\mu u_\nu + \frac{1}{2} b^2 g_{\mu\nu} - b_\mu b_\nu. \tag{15}$$

The four-velocity of matter is

$$u^\mu = \frac{dx^\mu}{ds} = \left\{u^t, u^r, u^\theta, u^\phi\right\} \tag{16}$$

and $\varepsilon = \rho + u_{\rm int} + p_{\rm gas}$ is the total mass-energy density, with ρ, $u_{\rm int}$, and $p_{\rm gas}$ being the matter density, internal energy, and pressure, and b^μ is the magnetic field four-vector. In the simulations, one solves the conservation equation

$$\nabla^\mu\, T^{\rm Tot}_{\mu\nu} = 0 \tag{17}$$

together with the material equations (equation of state), the induction equation for the magnetic field, and proper boundary conditions on the chosen metric background that defines the covariant derivative, ∇_μ. The continuity equation

$$\nabla_\mu (u^\mu \rho) = 0 \tag{18}$$

assures that matter is neither created nor destroyed during accretion.

The three simulations, L26, P13, and R25, mentioned in the present paper, were performed for accretion onto a non-rotating black hole described by the Schwarzschild metric, with $M = 10\,M_\odot$ for L26 (the other two used non-radiative GRMHD, which is scale-free). All are three-dimensional; P13 and R25 use an initial torus threaded by magnetic loops with opposite polarity, and the same prescription for cooling, substituting the radiative losses (Penna et al. 2010). Unfortunately, both of these simulations are rather short, with a total duration of about $20\,000\,GM/c^3$, and the time-averaged properties, including α, are only averaged over $5000\,GM/c^3$ for R25 and $13\,000\,GM/c^3$ for P13. During this short duration, the mass accretion rate is barely stable inside the averaging window. L26, on the other hand, is evolved for more than $80\,000\,GM/c^3$ and averaged over the last $17\,000\,GM/c^3$, with a stable mass accretion rate. This mainly affects the radial extent of the converged region of the simulations, which in the case of the short simulations covers only a few units of r_H above the radius $r_{\rm ISCO}$.

In contrast to the other two simulations, the puffy disc (L26) uses radiative GRMHD, where the gas conservatively exchanges energy and momentum with a frequency-integrated radiation field, a significantly more realistic approach. The non-radiative simulations use a cooling function to keep the accretion disc geometrically thin; thus, they omit radiation pressure, a crucial component for modelling the disc, and make a strong assumption about its structure.

The behaviour of the stress depends on local and quasi-local effects of the turbulence driven by the magnetorotational instability (MRI; Balbus & Hawley 1991) and on the global constraints given by the black hole geometry. It is natural to expect that the local effects are best described in the reference frame comoving with matter $e^\mu{}_{(k)}$ and the global constraints in the static reference frame attached to the space-time geometry $\tau^\mu{}_{[k]}$ (see Kulkarni et al. 2011, for the full formulation of this tetrad). The symbols $e^i{}_{(k)}$ and $\tau^i{}_{[k]}$ denote an orthonormal base of four-vectors:

$$e^\mu{}_{(t)} = \langle u^\mu \rangle_t, \quad \tau^\mu{}_{[t]} = n^\mu, \tag{19}$$

where $\langle u^\mu \rangle_t$ is time-averaged matter four-velocity (turbulence is smoothed out in time) and $n^\mu = \eta^\mu [(\eta\eta)]^{-1/2}$ is the four-velocity of the static observer (in the Schwarzschild case). An invariant formula for the stress adopted in L26 and P13 reads

$$\mathbb{T} = \langle T_{\mu\nu} e^\mu{}_{(r)}\, e^\nu{}_{(\phi)} \rangle_{t,\phi} = \langle T_{(r)(\phi)} \rangle_{t,\phi}, \tag{20}$$

where the angle-bracket subscripts label the averaging over time (t) and/or azimuth (ϕ).

The physical meaning of this formula is explained in P13, including the effects of different ways of averaging the simulation. This approach provides a frame of a quasi-stationary flow (mean comoving frame), allowing us to study the stress in a way similar to how it was defined in the Shakura & Sunyaev (1973) disc model. R25, on the other hand, calculates α using only the Maxwell stress in the local frame, defined by the instantaneous fluid velocity, which omits the Reynolds stress completely and only captures the instantaneous state of the fluid, rather than the quasi-stationary one.

[5] We set here G = c = M = 1 for simplicity.

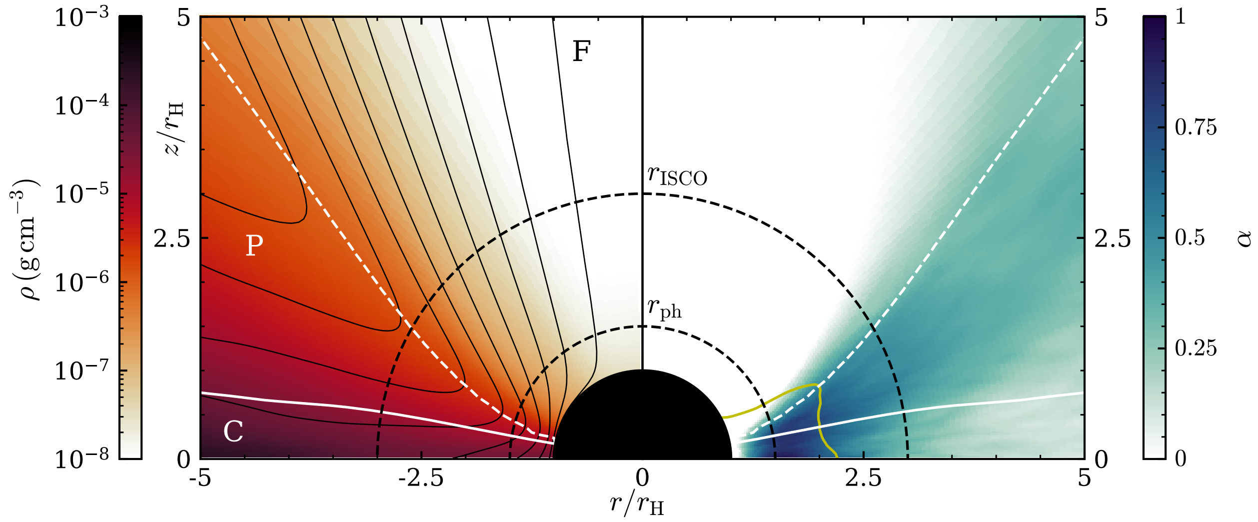

Fig. 2. This figure shows the time and azimuth-averaged structure of a puffy disc around our $M = 10\,\mathrm{M}_\odot$ black hole. There are three regions: C: dense core, P: puffy region, and F: funnel. *Left:* The colour map of gas density with the magnetic field lines in black contours. *Right*: Viscous α colour map, and the magnetosonic surface (yellow contour) defining the approximate separation between the plunging region and the rotating disc, which we use as the sonic point in this work. Note the increase in α in the plunging region. In both parts, the white dashed line indicates the photosphere, and the full line indicates the density scale height.

3.2. The puffy discs

Our puffy accretion discs are near-Eddington or mildly sub-Eddington, radiation pressure-dominated discs around stellar-mass non-rotating black holes, modelled using three-dimensional global radiative GRMHD simulations (Lančová et al. 2019; Sądowski 2016; L26). The calculations were performed using the KORAL code (Sądowski et al. 2013), and were designed so that the accretion disc self-consistently develops from a dense torus acting as a source of matter far from the central black hole. Puffy discs are stabilised against thermal instabilities, which are known to be critical in analytical radiation-pressure-dominated accretion discs, by a vertical net flux of magnetic field (Sądowski 2016; Oda et al. 2009; Mishra et al. 2022). The resulting disc is geometrically much thicker than any prediction of standard models allows, and so its observable properties are different from usual (Wielgus et al. 2022).

Here, in Figure 2, we present data from a simulation that reached a mass accretion rate of $\dot{m} = 0.6\,\dot{M}_{\rm Edd}$. The numerical methods and details can be found in L26. The structure of the disc, as shown in the left part of Figure 2, can be separated into two optically thick regions – the geometrically thin dense core (C) and the puffy region (P) – and is accompanied by an optically thin polar funnel (F) dominated by outflow. The core is defined by a scale-height, which is significantly different from that of the photosphere which encloses also the puffy region. The photospheric height of the disc is comparable to the radial distance from the centre ($H/r \sim 1$), whereas the standard disc models predict $H/r < 0.3$ for the same mass accretion rate. The puffy disc structure resembles a thin disc surrounded by a warm corona (Różańska et al. 2015; Gronkiewicz & Różańska 2020) but the puffy region also supplies most of the mass accretion, in comparison with the very low inflow in the central core.

3.3. The puffy disc stress calculations

In extracting α from the GRMHD simulations, L26 followed the method described in P13 for calculating the stress, which consists of three steps. First, one defines the time-averaged three-dimensional four-velocity, $\langle u^\mu\rangle_t = U^\mu$ and constructs the co-moving tetrad, $e^\nu_{(k)}$. Next, one calculates the total stress, with its Reynolds and Maxwell parts, as the tetrad $(r)(\phi)$ components of the corresponding stress-energy tensors computed from individual 3D snapshots and subsequently averaged over time and azimuth, $\langle T^{\rm Tot}_{(r)(\phi)}\rangle_{t,\phi}$, $\langle T^{\rm Rey}_{(r)(\phi)}\rangle_{t,\phi}$, $\langle T^{\rm Max}_{(r)(\phi)}\rangle_{t,\phi}$, according to Eq. (20). The density-weighted vertically averaged stress and its components are shown in Figure 3. Finally, α is obtained from

$$\alpha = \frac{\mathbb{T}}{\langle p\rangle_{t,\phi}}, \tag{21}$$

in both L26 and P13, where $\langle p\rangle_{t,\phi}$ is the averaged total pressure. Then, a radial profile of α is obtained by a density-weighted average of the two-dimensional α map (shown in the right half of Figure 2) in the vertical direction. L26 included the gas, magnetic, and radiation pressures for the α calculations, $p = p_{\rm gas} + p_{\rm mag} + p_{\rm rad}$. This is in contrast with P13, who used only the magnetic and gas pressures, $p = p_{\rm gas} + p_{\rm mag}$, since their simulations do not provide the radiation pressure component. R25 further used only the instantaneous fluid frame Maxwell stress and gas and magnetic pressure.

4. Fundamental stress properties

In this paper, we report that the results of GRMHD simulations of the black hole accretion disc obtained in several independent studies by different authors seem to indicate a universal radial dependence of the Shakura-Sunyaev α-viscosity coefficient, which most probably reflects fundamental properties of the stress itself. This finding suggests two directions of future research: first, an explanation from first principles of the universal stress behaviour seen in Figure 3, and second, an application of our α-viscosity formula (Eq. (11)) to construct semi-analytic models of thin and slim discs.

We will discuss the fundamental physical reasons for such behaviour in a forthcoming, much more mathematically minded

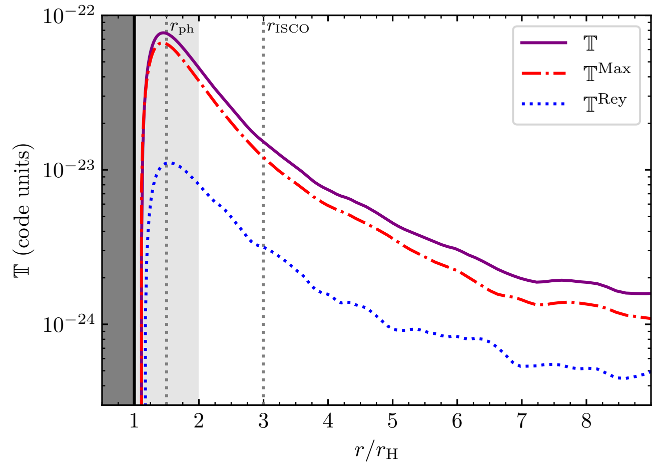

Fig. 3. Behaviour of the total stress $\mathbb{T} = \mathbb{T}^{\rm Max} + \mathbb{T}^{\rm Rey}$ and its Reynolds and Maxwell components (the curves shown are taken from L26): the stress is zero at the horizon, it has a maximum at the circular photon orbit and is much smaller far away than in the plunging region. The behaviour of the stress is remarkably similar to the behaviour of the inverse of the square of the 'gyration radius', $\tilde{r}$.

publication. In this section, we only briefly hint at some relevant points, appealing to physical intuition rather than giving solid mathematical proofs. One of the issues that we will carefully clarify (because it is often a source of confusion) is that the stress is here zero at the horizon, even though the equivalence principle assures that one cannot know from local measurements if the horizon is being crossed. In a wider context: the MRI builds the stress locally, in the comoving frames, but some of the stress properties reflect the global aspects of the black hole space-time.

4.1. Stress is zero at the horizon

Let us cast Eq. (2) in the form

$$\mathbb{T} = \dot{J} - \langle \dot{M} \rangle \langle j \rangle \tag{22}$$

which underlines the physical meaning of the stress: it represents the part of the angular momentum flux through a surface $\mathcal{S}$ that is not carried with the mean mass accretion flux, $\langle \dot{M} \rangle \langle j \rangle$. Here $\langle j \rangle$ is the mean specific angular momentum at $\mathcal{S}$. Abramowicz et al. (2010) applied Eq. (22) and argued that when a sphere $\mathcal{S}$ of radius r in an accretion disc is crossed by a 'mean' accretion flow, $\langle \dot{M} \rangle$, in the + direction (towards the black hole), turbulence causes an additional (fluctuating) downstream flux $\delta \dot{M}^+$, and an upstream flux $\delta \dot{M}^-$, and so the total fluxes of mass in the + and − directions are $\dot{M}^+ = \langle \dot{M} \rangle + \delta \dot{M}^+$ and $\dot{M}^- = \delta \dot{M}^-$. Therefore,

$$\mathbb{T} = \frac{1}{2}(\delta \dot{M}^-)(\delta j), \tag{23}$$

where $(\delta j) = [\dot{M}^+ j^+ - \dot{M}^- j^-]/\langle \dot{M} \rangle$.

From Eq. (23), Abramowicz et al. (2010) deduced that, if the surface ($\mathcal{S}$) coincides with the black hole horizon, then no upstream flux of mass exists, ($\delta \dot{M}^- = 0$), and hence there is no stress at $r = r_{\rm H}$. This simple argument, which captures the essence of the relevant physics, was later extended by Lasota et al. (2014) who considered an arbitrary stress-energy tensor ($T_{\mu\nu}$), that describes any kind of matter or field, in particular the electromagnetic field. Specifically, for the electromagnetic field in the GRMHD environment, Lasota et al. (2014) rigorously proved that the Blandford-Znajek mechanism is an electromagnetic version of the Penrose process. They showed that, although angular momentum is transported along the field lines of a strongly enhanced magnetic field, no magnetic stress (torque) is exerted at the horizon. Instead, the black hole absorbs negative energy and negative angular momentum, resulting in a reduction of its rotational energy. As a particular example, Lasota et al. (2014) showed that this general principle ('no stress but negative energy absorption') takes place in magnetically arrested accretion discs (Bisnovatyi-Kogan & Ruzmaikin 1974; Narayan et al. 2003).

The vanishing of the turbulent stress in the mean comoving frame at the horizon, which we use in the definition of viscous α, cannot be directly linked only to crossing the horizon: by the equivalence principle, a local comoving observer does not recognise the horizon crossing. Nonetheless, GRMHD simulations show that the flow at the horizon is nearly laminar and almost radial. One reason for this is that once the radial motion becomes highly supersonic and super-Alfvènic, the MRI stops being an efficient driver of turbulence, and both the turbulent Reynolds and Maxwell stresses decay quickly. While the Reynolds stress calculated in the GRMHD simulations discussed here is the turbulent one, the Maxwell stress in the plunging region is mainly due to the large-scale magnetic field. However, when the azimuthal component of the mean magnetic field becomes negligible in the ideal MHD (magneto-hydrodynamic) flow due to the field lines being frozen into the radially infalling fluid, the relevant component of the Maxwell stress also vanishes.

4.2. Stress has its maximum at the photon radius

Figure 3 shows that GRMHD simulations clearly indicate that both the Reynolds and Maxwell components of the stress (and therefore also the total stress) peak sharply at the location of the radius of the circular photon orbit. In a forthcoming analytic study we plan to address the question of whether the stress maximum is caused by the reversal of the sense of outward and inward radial directions that is known to occur at the location of the circular photon orbit $r_{\rm ph} = (3/2)r_{\rm H}$. For $r < r_{\rm ph}$, 'out' points towards the black hole at the centre (Abramowicz et al. 1995; Abramowicz & Prasanna 1990). The reversal influences all of the dynamical properties of rotation; in particular, the reversed Rayleigh criterion demands that, for stability, angular momentum should increase inwards, meaning towards the black hole. Correspondingly, the Rayleigh stress transports angular momentum inwards, into the black hole (Anderson & Lemos 1988). There are several other examples of this reversal described in a popular Scientific American article by Abramowicz (1993). The reversal of the dynamical sense of the outward and inward directions could be another reason for decreasing stresses close to the horizon, discussed in the previous subsection. As this purely geometric effect causes a shear reversal, one may speculate that the reversed shear suppresses the MRI and causes the turbulent stress to vanish.

According to our proposed prescription given in Eq. (11), $\alpha(r)$ reaches maximum exactly at the photon orbit. However, our argumentation pertains to the behaviour of stress rather than α, which is proportional to stress and inversely proportional to pressure. The radial behaviour of the stress, with a maximum located exactly at the photon orbit, is shown in Figure 3. The small shift of the maximum of $\alpha(r)$ away from the photon orbit, as seen in Figure 1, is then caused by the radial dependence of pressure. Neglecting this small shift in our prescription and framing the discussion around α is motivated by historical and practical reasons, related to applications for modelling of accretion discs.

4.3. At large radii α = (shear)/(vorticity)

In the far region where $r \gg r_{\rm H}$

$$\alpha \approx \alpha_\infty = \text{const}, \tag{24}$$

with $10^{-2} \lesssim \alpha_\infty \lesssim 10^{-1}$. Abramowicz et al. (1996) noticed that in the far region, for flows that are dominated by matter spiralling down along orbits that may be considered almost circular, a more detailed fitting is consistent with

$$\alpha \approx \frac{\alpha_\infty}{3}\left(\frac{\sigma}{\omega}\right), \tag{25}$$

where the kinematic invariants shear = σ and vorticity = ω are given in the Schwarzschild space-time by

$$\sigma^2 = -\frac{1}{4}\,(1-\Omega j)^{-2}(\tilde{r})^{+2}(\nabla^\mu\Omega)(\nabla_\mu\Omega), \tag{26}$$

$$\omega^2 = -\frac{1}{4}\,(1-\Omega j)^{-2}(\tilde{r})^{-2}(\nabla^\mu j)(\nabla_\mu j). \tag{27}$$

This possibly reflects the origin of the stress as driven by the local MRI, with turbulence being sensitive to local gradients of angular velocity (Ω) and specific angular momentum (j).

The numerical results of Abramowicz et al. (1996) for stratified MRI turbulence were verified by Hawley et al. (1999), who considered unstratified MRI turbulence for a fine mesh of shear parameters, q. In their local shearing box simulations, $q = -d\ln\Omega/d\ln r$ is the double-logarithmic angular velocity gradient, which quantifies the strain of the background velocity Ω_0, $\sigma = q\Omega_0/\sqrt{2}$. By contrast, the vorticity of the background velocity is $\omega = r^{-1}d(r^2\Omega/dr)/\sqrt{2} = (2-q)\Omega_0/\sqrt{2}$. Hawley et al. (1999) noted that for small values of q, the turbulent fluctuations in the stress are dominated by the magnetic contributions. Interestingly, based on their analytical considerations, they also pointed out that the magnetic stress fluctuations couple directly to the strain $\sigma \propto q$, while the kinetic stress fluctuations couple to the vorticity $\omega \propto 2-q$. Therefore, $\sigma/\omega = q/(2-q)$, so for small values of q, the vorticity $\omega \propto 2-q$ limits the turbulent transport quantified by α, while strain $\sigma \propto q$ promotes it.

These results were subsequently corroborated by Pessah et al. (2006, 2008) using a linear stability analysis. In particular, they confirmed the observation that the turbulent stresses are not simply proportional to the local shear, as one might have naively expected. Similar conclusions were also drawn by Liljeström et al. (2009) using a closure model of Ogilvie (2003). The numerical results of Abramowicz et al. (1996) and Hawley et al. (1999) were later also confirmed for much taller shearing boxes of up to eight scale heights (Nauman & Blackman 2015).

5. Conclusions

We have suggested an improvement to the well-known analytic Shakura-Sunyaev α-prescription for the stress $\mathbb{T} = \alpha p$. Instead of the original ansatz α = const, we propose

$$\alpha = \alpha_P\,(r_{\rm H}/\tilde{r})^2 + \alpha_\infty\,(\eta\eta)\,, \quad \tilde{r}^2 = -\frac{(\xi\xi)}{(\eta\eta)}, \tag{28}$$

with $\alpha_P \sim 1$ and $\alpha_\infty \sim 0.01$ being phenomenological constants and $r_{\rm H} = 2GM/c^2$ being the non-rotating black hole horizon radius.

The values of α_P and α_∞ can be connected to the values used in standard disc modelling (e.g. $\alpha_\infty \sim 0.1$) and to the magnetisation of the matter in the innermost region, for example through scaling $\alpha = 0.5\beta^{-1}$, where β is the ratio of thermal to magnetic pressure (Sorathia et al. 2012). A more detailed investigation of how disc properties and magnetisation affect the shape of the $\alpha(r)$ profile is left for future work. However, in L26 we showed that the α behaviour does not vary significantly for simulations covering the mass accretion rate range $\dot{m} = 0.4$–$0.9\,\dot{M}_{\rm Edd}$. Simulations by P13 and R25 were performed for lower mass-accretion rates and lower disc magnetisation and show lower peak α values (see the caption of Figure 1), but our formula fits those results well with different values of the α_P and α_∞ parameters.

The proposed analytic formula is based on the results of GRMHD simulations that describe black hole accretion discs with sub-Eddington and near-Eddington accretion rates. It is analytic and expressed in terms of coordinate-independent quantities – the Kerr metric Killing vectors η^μ and ξ^μ. It is short, simple, and explicit in any of the specific coordinates used in black hole accretion studies. It accurately embraces fundamental properties of the stress in curved black hole space-time: the stress is zero at the event horizon, it is smaller far away from the black hole than in the plunging region closer to it, and it peaks near to the location of the circular light radius.

We plan to use Eq. (28) to calculate improved models of both stationary and non-stationary slim accretion discs. For the stationary ones, we will first need to convert the equations given by Sądowski (2009) into the comoving frame so as to ensure that the stress description Eq. (28) corresponds directly to that used in L26 and other GRMHD simulations. For the non-stationary ones, the simulations by Szuszkiewicz & Miller (1998) and Szuszkiewicz & Miller (2001) have already been performed in a comoving frame; further work will involve applying Eq. (28) within a similar scheme but with modifications to give an improved relativistic treatment of the accretion flow between the sonic radius and the black hole horizon, enabling it to follow the essential characteristics of the flow there. This approach should make it possible to calculate long-time evolution of the disc, as before, which is crucial for understanding the observational appearance of objects powered by accretion onto black holes.

The most exciting research outcome that one may anticipate from the findings of this paper is the possibility of explaining these features of the stress:

$$\mathbb{T}(r_{\rm H}) = 0, \quad \mathbb{T}(r_{\rm ph}) = \mathbb{T}_{\max}, \quad \mathbb{T}(r \gg r_{\rm H}) \propto \sigma/\omega,$$

which could reflect the way in which the quasi-local MRI turbulence interacts with the global constraints coming from the space-time geometry of the black hole.

This paper is an initial attempt to extract useful information about the stress in accretion discs around black holes from the numerical results of recent GRMHD simulations. We point out that the radial stress profiles from three independent and quite different numerical simulations return a very similar profile, and this is our motivation for proposing its 'universal' character: (1) the stress measured in the comoving frame is zero at the black hole horizon and (2) it has a maximum at the location of the circular photon orbit.

Of course, as these statements are based on numerical results, one may have doubts about whether the zero point of the stress really occurs exactly at the horizon. It would be very desirable to have an analytic investigation of this – and we are working on that. The same concerns the need to have equivalent results for rotating black holes in the hope of finding a more universal solution.

There are currently very few available GRMHD simulations of accretion onto a spinning Kerr black hole in a regime where the α-viscosity prescription is applicable in analytical modelling, and even fewer radiative GRMHD simulations where the results are not affected by the choice of cooling function or disc instabilities, and where it is possible to study the flow properties in the innermost regions around the black hole (e.g., Fragile et al. 2023; Zhang et al. 2026, and others). We aim to explore this regime with puffy disc simulations in the future. In any case, exploring the parameter space of various black hole masses, spins, and mass accretion rates would be extremely computationally expensive, and hence analytic studies are very much needed here.

The most obvious astrophysical applications of our paper are to construct analytic and semi-analytic models of accretion with the aid of the new viscosity prescription, particularly for slim discs. However, these studies may give results that would be far more general than the astrophysical accretion disc theory itself: for example, that the stress profile, independently of the nature of the stress, is shaped near to the horizon mainly by gravity, and not by properties of the fluid.

Acknowledgements. We are grateful to the anonymous referee for valuable suggestions. The first version of this draft was prepared at the RAGtime workshop in Opava. MA and JH acknowledge the Czech Science Foundation (GAČR) grant No. 21-06825X, and DL project No. 25-16928O. AB acknowledges support by the Swedish Research Council (Vetenskapsrådet) under grant No. 2025-05957. JM acknowledges continuing support from the Italian Istituto Nazionale Previdenza Sociale and provision of facilities by the University of Oxford. MW is supported by a Ramón y Cajal grant RYC2023-042988-I from the Spanish Ministry of Science and Innovation and acknowledges financial support from the Severo Ochoa grant CEX2021-001131-S funded by MCIN/AEI/10.13039/501100011033. This work was supported by the Ministry of Education, Youth and Sports of the Czech Republic through the e-INFRA CZ (ID:90254). *Data availability.* The simulation data underlying this article are available upon reasonable request to the corresponding authors.

References

Abramowicz, M. A. 1993, Sci. Am., 268, 74
Abramowicz, M. A., & Prasanna, A. R. 1990, MNRAS, 245, 720
Abramowicz, M. A., Czerny, B., Lasota, J. P., & Szuszkiewicz, E. 1988, ApJ, 332, 646
Abramowicz, M. A., Miller, J. C., & Stuchlík, Z. 1993, Phys. Rev. D, 47, 1440
Abramowicz, M. A., Nurowski, P., & Wex, N. 1995, Class. Quant. Grav., 12, 1467
Abramowicz, M., Brandenburg, A., & Lasota, J.-P. 1996, MNRAS, 281, L21
Abramowicz, M. A., Jaroszyński, M., Kato, S., et al. 2010, A&A, 521, A15
Anderson, M. R., & Lemos, J. P. S. 1988, MNRAS, 233, 489
Balbus, S. A., & Hawley, J. F. 1991, ApJ, 376, 214
Bisnovatyi-Kogan, G. S., & Ruzmaikin, A. A. 1974, Ap&SS, 28, 45
Dhang, P., Dexter, J., & Begelman, M. C. 2025, ApJ, 980, 203
Fragile, P. C., Anninos, P., Roth, N., & Mishra, B. 2023, ApJ, 959, 59
Gronkiewicz, D., & Różańska, A. 2020, A&A, 633, A35
Hankla, A. M., Scepi, N., & Dexter, J. 2022, MNRAS, 515, 775
Hawley, J. F., Balbus, S. A., & Winters, W. F. 1999, ApJ, 518, 394
Krolik, J. H., & Hawley, J. F. 2002, ApJ, 573, 754
Kulkarni, A. K., Penna, R. F., Shcherbakov, R. V., et al. 2011, MNRAS, 414, 1183
Lančová, D., Abarca, D., Kluźniak, W., et al. 2019, ApJ, 884, L37
Lančová, D., Wielgus, M., Abramowicz, M., et al. 2026, MNRAS, 550, stag1278
Lasota, J.-P., Gourgoulhon, E., Abramowicz, M., Tchekhovskoy, A., & Narayan, R. 2014, Phys. Rev. D, 89, 024041
Liljeström, A. J., Korpi, M. J., Käpylä, P. J., Brandenburg, A., & Lyra, W. 2009, Astron. Nachr., 330, 92
Mishra, B., Fragile, P. C., Anderson, J., et al. 2022, ApJ, 939, 31
Morales Teixeira, D., Avara, M. J., & McKinney, J. C. 2018, MNRAS, 480, 3547
Mummery, A., & Balbus, S. 2023, MNRAS, 521, 2439
Mummery, A., Jiang, J., Ingram, A., Fabian, A., & Rule, J. 2025, MNRAS, 544, 2880
Narayan, R., Igumenshchev, I. V., & Abramowicz, M. A. 2003, PASJ, 55, L69
Nauman, F., & Blackman, E. G. 2015, MNRAS, 446, 2102
Novikov, I. D., & Thorne, K. S. 1973, in Black Holes (Les Astres Occlus), eds. C. Dewitt, & B. S. Dewitt, 343
Oda, H., Machida, M., Nakamura, K. E., & Matsumoto, R. 2009, ApJ, 697, 16
Ogilvie, G. I. 2003, MNRAS, 340, 969
Penna, R. F., McKinney, J. C., Narayan, R., et al. 2010, MNRAS, 408, 752
Penna, R. F., Sądowski, A., Kulkarni, A. K., & Narayan, R. 2013, MNRAS, 428, 2255
Pessah, M. E., Chan, C.-K., & Psaltis, D. 2006, Phys. Rev. Lett., 97, 221103
Pessah, M. E., Chan, C.-K., & Psaltis, D. 2008, MNRAS, 383, 683
Reynolds, C. S. 2021, ARA&A, 59, 117
Różańska, A., Malzac, J., Belmont, R., Czerny, B., & Petrucci, P.-O. 2015, A&A, 580, A77
Rule, J., Mummery, A., Balbus, S., Stone, J. M., & Zhang, L. 2025, MNRAS, 542, 377
Sądowski, A. 2009, ApJS, 183, 171
Sądowski, A. 2016, MNRAS, 459, 4397
Sądowski, A., Narayan, R., Tchekhovskoy, A., & Zhu, Y. 2013, MNRAS, 429, 3533
Shafee, R., McKinney, J. C., Narayan, R., et al. 2008, ApJ, 687, L25
Shakura, N. I., & Sunyaev, R. A. 1973, A&A, 24, 337
Sorathia, K. A., Reynolds, C. S., Stone, J. M., & Beckwith, K. 2012, ApJ, 749, 189
Szuszkiewicz, E., & Miller, J. C. 1998, MNRAS, 298, 888
Szuszkiewicz, E., & Miller, J. C. 2001, MNRAS, 328, 36
Wielgus, M., Lančová, D., Straub, O., et al. 2022, MNRAS, 514, 780
Zdziarski, A. A., Marcel, G., Veledina, A., Olejak, A., & Lančová, D. 2026, New A Rev., 102, 101746
Zhang, L., Stone, J. M., Davis, S. W., et al. 2026, arXiv e-prints [arXiv:2603.05588]

Appendix A: Kerr metric formulae

The covariant definitions of the quantities used in the paper are given in terms of Kerr metric symmetry generators: the Killing vector of time symmetry η^i and the Killing vector of axial symmetry ξ^i. The Killing vectors obey

$$\nabla_{(i}\eta_{k)} = 0, \quad \nabla_{(i}\xi_{k)} = 0, \quad \eta^i \nabla_i \xi_k = \xi^i \nabla_i \eta_k. \tag{A.1}$$

The frame dragging ω and the gravity potential Φ obey

$$\omega = -\frac{(\eta\xi)}{(\xi\xi)}, \quad \Phi = -\frac{1}{2}\ln\left[(\eta\eta) + 2\omega\,(\eta\xi) + \omega^2(\xi\xi)\right] \tag{A.2}$$

which help to define the four-velocity of the stationary observer (ZAMO)

$$n^i = e^{\Phi}(\eta^i + \omega\xi^i), \quad (nn) = 1. \tag{A.3}$$

A circular motion at the equatorial plane symmetry of the Kerr metric is defined by writing two equivalent expressions for the four-velocity of matter,

$$u^i = A(\eta^i + \Omega\xi^i), \quad A^{-2} = (\eta\eta) + 2\Omega\,(\eta\xi) + \Omega^2(\xi\xi), \tag{A.4}$$

$$u^i = \gamma(n^i + v\tau^i), \quad \tau^i = \xi^i/r, \quad r^2 = -(\xi\xi). \tag{A.5}$$

These equations invariantly define the angular velocity Ω, the orbital velocity v and the redshift factor $\gamma^{-2} = 1 - v^2$. The specific angular momentum j obeys

$$j = -\frac{(u\xi)}{(u\eta)}, \quad j = v\tilde{r} = \tilde{\Omega}\tilde{r}^2, \tag{A.6}$$

where $\tilde{\Omega} = \Omega - \omega$ and

$$\tilde{r} = re^{\Phi} \tag{A.7}$$

is the gyration radius; see Abramowicz et al. (1995) for more details.